

DISCOVERY OF A YOUNG, ENERGETIC 70.5 MS PULSAR ASSOCIATED WITH THE TEV GAMMA-RAY SOURCE HESS J1837–069

E. V. GOTTHELF & J. P. HALPERN

Columbia Astrophysics Laboratory, Columbia University, 550 West 120th Street, New York, NY 10027, USA

To Appear in *The Astrophysical Journal*

ABSTRACT

We report the discovery of 70.5 ms pulsations from the X-ray source AX J1838.0–0655 using the *Rossi X-ray Timing Explorer (RXTE)*. PSR J1838–0655 is a rotation-powered pulsar with spin-down luminosity $\dot{E} = 5.5 \times 10^{36}$ ergs s^{−1}, characteristic age $\tau_c \equiv P/2\dot{P} = 23$ kyr, and surface dipole magnetic field strength $B_s = 1.9 \times 10^{12}$ G. It coincides with an unresolved *INTEGRAL* source and the extended TeV source HESS J1837–069. At an assumed distance of 6.6 kpc by association with an adjacent massive star cluster, the efficiency of PSR J1838–0655 converting spin-down luminosity to radiation is 0.8% for the 2–10 keV *ASCA* flux, 9% for the 20–300 keV *INTEGRAL* flux and $\sim 3\%$ for the > 200 GeV emission of HESS J1837–069, making it a plausible power source for the latter. A *Chandra* X-ray observation resolves AX J1838.0–0655 into a bright point source surrounded by a $\approx 2'$ diameter, centrally peaked nebula. The spectra of the pulsar and nebula are each well fitted by power laws, with photon indices $\Gamma = 0.5(0.3–0.7)$ and $\Gamma = 1.6(1.1–2.0)$, respectively. The 2–10 keV X-ray luminosities of the pulsar and nebula are $L_{PSR} = 4.6 \times 10^{34} d_{6.6}^2$ ergs s^{−1} and $L_{PWN} = 5.2 \times 10^{33} d_{6.6}^2$ ergs s^{−1}. A second X-ray source adjacent to the TeV emission, AX J1837.3–0652, is resolved into an apparent pulsar/PWN; it may also contribute to HESS J1837–069. The star cluster RSGC1 may have given birth to one or both pulsars, while fueling TeV emission from the extended PWN with target photons for inverse Compton scattering.

Subject headings: pulsars: individual (AX J1838.0–0655, AX J1837.3–0652, PSR J1838–0655) — stars: neutron — supernova remnants — X-rays: stars

1. INTRODUCTION

Surveys of the Galactic plane (Aharonian et al. 2006a) by the High Energy Stereoscopic System (H.E.S.S.) find that at least half of its sources (Funk 2007) can be identified with supernova remnants (SNRs) or pulsar wind nebulae (PWNe). The sizes of those sources that are identified as PWNe are generally larger in TeV γ -rays than in X-rays, revealing a new view of the penetration of high-energy particles into the surrounding medium. The larger TeV nebulae are often displaced from the pulsar, possibly by the reverse shock of a supernova that exploded in an inhomogeneous medium. They may also contain relic electrons from the more energetic, younger phase of the pulsar spin-down. The characteristic mismatch between X-ray and γ -ray sizes, together with the positional offsets of the X-ray and TeV emitting nebulae, are becoming familiar as new examples are found (Aharonian et al. 2006b, 2006c, 2007). Understanding exactly how the spin-down luminosity of a particular pulsar powers its TeV nebula requires time-dependent modeling and sometimes uncertain details of the local environment that must be determined at other wavelengths. The favored theoretical mechanisms, either inverse-Compton scattering of ambient photons, or decay of neutral pions produced in hadronic collisions of high-energy protons with a dense phase of the ISM, are being tested in several cases. For a recent review of these issues, see de Jager & Djannati-Atai (2008).

A most instructive association is AX J1838.0–0655 with HESS J1837–069. One of the first extended sources detected by H.E.S.S. (Aharonian et al. 2005, 2006a), it was considered unidentified until now even though X-ray

studies of the field pointed to a coincident hard, steady X-ray source detected up to 300 keV by *INTEGRAL* (Malizia et al. 2005). AX J1838.0–0655 was seen by X-ray satellites spanning decades, beginning with *Einstein* (1E 1835.3–0658; Hertz & Grindlay 1988), and including *ASCA* (Bamba et al. 2003), *BeppoSAX* (Malizia et al. 2005), *XMM-Newton* (unpublished), and *Swift* (Landi et al. 2006), always with steady flux. Bamba et al. (2003) measured 1.1×10^{-11} ergs cm^{−2} s^{−1} from AX J1838.0–0655 in the 0.7–10 keV band, which is comparable to the > 200 GeV flux from HESS J1837–069, 3.3×10^{-11} ergs cm^{−2} s^{−1} (Aharonian et al. 2006a). The absence of variability is an important clue to the nature of AX J1838.0–0655, as is its hard spectrum. Malizia et al. (2005) fitted the combined *INTEGRAL* and *ASCA* spectrum with a power law of photon index $\Gamma = 1.5$, and conjectured that the source is a supernova product, more likely a PWN than a shell SNR.

In §2 we describe our analysis of a *Chandra* image of HESS J1837–069 that resolves AX J1838.0–0655 into a pulsar/PWN, and study its spectral properties. We also address the nature of the other X-ray sources in the vicinity of HESS J1837–069, one of which, AX J1837.3–0652, is evidently a second PWN. Motivated by the *Chandra* results, we proposed observations of AX J1838.0–0655 with *RXTE* to search for its putative pulsar. The resulting discovery of PSR J1838–0655 and measurement of its spin-down parameters are described in §3. We show that the rotational energy/spin-down luminosity of PSR J1838–0655 are sufficient to power the TeV emission of HESS J1837–069, and we further argue in §4 that the adjacent massive star cluster RSGC1 (Figer et al. 2006; Davies et al. 2008) provides

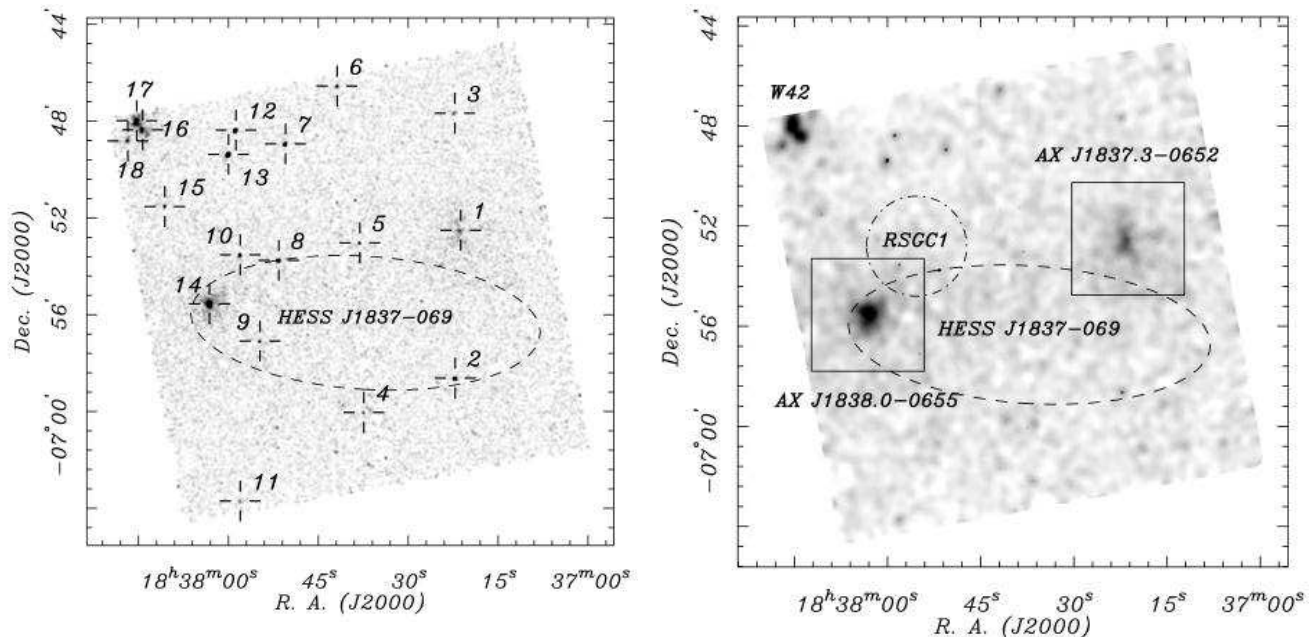


FIG. 1.— *Chandra* ACIS-I broad-band X-ray image of HESS J1837–069. *Left*: Image scaled to emphasize point sources listed in Table 1. *Right*: Image smoothed to emphasize diffuse emission. The ellipse represents the two-dimensional Gaussian 1σ extent of the TeV emission (Aharonian et al. 2006a). The circle is the approximate extent of the red supergiant cluster RSGC1 (Figer et al. 2006). The squares indicate the zoomed-in regions around AX J1838.0–0655 and AX J1837.3–0652 corresponding to the insets in Figure 2.

ambient target photons for inverse Compton scattered TeV emission by PWN electrons from AX J1838.0–0655 and possibly from AX J1837.3–0652, whose pulsar may also have been born in the cluster.

2. CHANDRA OBSERVATIONS AND RESULTS

A 20 ks *Chandra* X-ray observation of HESS J1837–069 was made on 2006 August 19 UT using the Advanced CCD Imaging Spectrometer (ACIS; Burke et al. 1997) operating in the full-frame TIMED/VFAINT exposure mode. This detector is sensitive to X-rays in the 0.3–12.0 keV energy range with a resolution of $\Delta E/E \sim 0.06$ FWHM at 1 keV. The imaging system offers an on-axis spatial resolution of $\approx 0.5''$, which is also the instrument pixel size, and increases to $\sim 5''$ at $10'$ off-axis. A total of 19.9 ks of live-time was accumulated with a CCD frame time of 3.241 s (given the 1.3% readout deadtime). With a maximum count rate in a pixel of $< 0.004 \text{ s}^{-1}$, photon pile-up can safely be ignored. As normal procedure, the spacecraft was dithered to average out the single-pixel spectral response. We used the standard processed and filtered event data. No time filtering was necessary as the background rate was stable over the course of the observation. All data reduction and analysis was performed using the CIAO (V3.4), FOOLS (V6.0.4), CALDB 3.4.2, and XSPEC (V12.2.1) X-ray analysis software packages. We followed the CIAO online science thread to create the exposure-corrected image.

Figure 1 is the exposure-corrected map of the entire 4-CCD ACIS-I field that is smoothed on two scales to highlight either the point sources or the diffuse emission. There are 18 unambiguous point sources (listed in Table 1); two of these, sources 1 and 14, have associated X-ray nebulae. Since the image was centered on the TeV emission, AX J1838.0–0655 (source 14) fell $5.25'$ off-axis,

near the gap between ACIS-I CCDs. Fortunately, exposure correction using the spacecraft dithering information fully recovers the fluxed image, allowing us to generate an accurate spectrum and radial profile.

2.1. AX J1838.0–0655

Figure 1 shows that AX J1838.0–0655 falls along the long axis of the TeV extent¹. Considering the off-axis location of the point source, we determine its precise location by fitting the off-axis point spread function following the CIAO recipe. Then, by registering other X-ray point sources with their optical or radio counterparts (see Table 1) we are able to refine the location of the point source in AX J1838.0–0655 to (J2000.0) R.A. = $18^{\text{h}}38^{\text{m}}03.13^{\text{s}}$, decl. = $-06^{\circ}55'33.4''$ with a 1σ error radius of $\approx 0.3''$. (A correction of $-0.55''$ in R.A. and $-0.09''$ in decl. was applied.)

Figure 2 shows an enlarged region of the *Chandra* image of AX J1838.0–0655, and its radial profile, clearly resolving a nebula from a point source. For spectral analysis of AX J1838.0–0655 we extract photons in the 2–10 keV energy band, below which the spectra are highly attenuated by the large column density. For the point-source spectrum, we extract 2124 photons from a $5'' \times 7''$ elliptical aperture centered on the source peak; the diffuse emission contributes a negligible background (21 counts) in this region. For the nebula we use a $1'$ radius extraction region, offset from the point source and centered at (J2000.0) R.A. = $18^{\text{h}}38^{\text{m}}03.1^{\text{s}}$, decl. = $-06^{\circ}55'40''$ with a $7'' \times 9''$ region around the pulsar removed. The background for the nebula was extracted

¹ Figure 6 of Landi et al. (2006) that graphs the TeV extent on the *Swift* X-ray image has the wrong position angle for the ellipse, which doesn't do justice to the case for association. We reproduce here the orientation given by Aharonian et al. (2006a).

TABLE 1
POINT SOURCES IN *Chandra* ACIS-I OBSID 6719

No.	X-ray Position		Counts	HR ^a	Optical ^b or Radio Position		B_2^b (mag)	R_2^b (mag)	ID (Spectral Type)
	R.A. (J2000)	Decl. (J2000)			R.A. (J2000)	Decl. (J2000)			
1....	18 37 21.21	−06 52 30.6	17	+0.77	AX J1837.3–0652
2....	18 37 22.14	−06 58 37.5	83	−0.36	18 37 22.126	−06 58 38.09	16.73	14.30	...
3....	18 37 22.20	−06 47 40.4	59	+0.82
4....	18 37 37.37	−07 00 02.6	19	−0.58	18 37 37.374	−07 00 02.47	16.50	13.64	...
5....	18 37 38.04	−06 53 01.8	25	+0.92
6....	18 37 41.84	−06 46 33.0	45	+0.86
7....	18 37 50.45	−06 48 56.4	85	+0.98	18 37 50.45	−06 48 56.9	GPSR5 25.320–0.098
8....	18 37 51.57	−06 53 45.4	274	+0.99	18 37 51.60	−06 53 45.0	GPSR5 25.252–0.139
9....	18 37 54.71	−06 57 05.6	23	+0.91
10...	18 37 58.00	−06 53 31.6	55	+0.96	18 37 57.99	−06 53 31.0	GPSR5 25.266–0.161
11...	18 37 58.00	−07 03 42.4	44	+0.85
12...	18 37 58.72	−06 48 22.5	129	−0.87	18 37 58.760	−06 48 22.39	8.76	7.75	HD 171999 (G5)
13...	18 37 59.97	−06 49 22.4	285	+0.96	Swift J1837.9–0649
14...	18 38 03.13	−06 55 33.4	2114	+0.92	AX J1838.0–0655
15...	18 38 10.59	−06 51 31.9	46	+0.80
16...	18 38 14.26	−06 48 21.7	240	+0.65
17...	18 38 15.27	−06 47 58.9	291	+0.42	18 38 15.231	−06 47 58.78	...	16.06	W42 1 (O5.5)
18...	18 38 16.75	−06 48 49.4	126	−0.06

NOTE. — Includes all point sources that have signal-to-noise ratio > 3 in the 0.3–10 keV band, as determined by the CIAO software package source-detection tool *wavdetect*. Units of right ascension are hours, minutes, and seconds, and units of declination are degrees, arcminutes, and arcseconds.

^aHardness ratio defined as $HR = (N_h - N_s)/(N_h + N_s)$, where N_s and N_h are the counts measured in the 0.3–2 keV and 2–10 keV energy band, respectively.

^bOptical data from the USNO-B1.0 catalog (Monet et al. 2003).

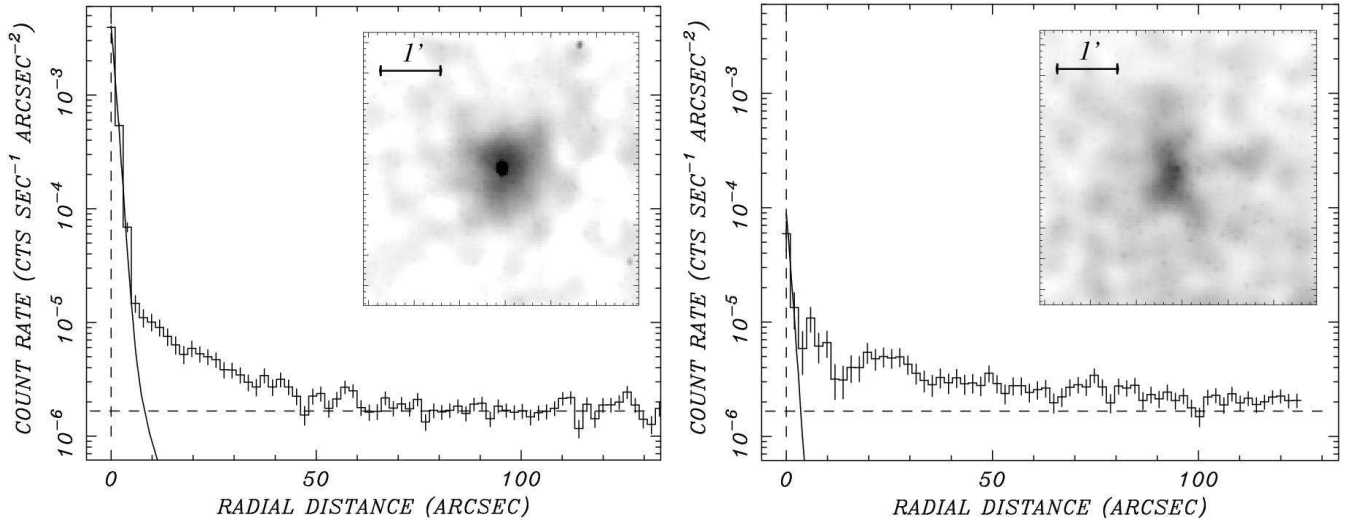


FIG. 2.— *Chandra* ACIS radial profiles of AX J1838.0–0655 (left) and AX J1837.3–0652 (right) compared to the scaled point spread function at their locations (FWHM $\approx 2''$; solid line). Surrounding each point source, a clear flux excess is evident over the field background flux level (horizontal dashed line) to $r \approx 60''$ in the case of AX J1838.0–0655. For AX J1837.3–0652, a larger but lower surface brightness extension is seen. Insets: Zoom-in on the *Chandra* images. The intensity is scaled to highlight the diffuse emission; the point sources are saturated.

from a concentric annulus of radii $1' < r \leq 2'$. The nebula so extracted comprises 483 photons after subtracting background (33%) and excising the point source.

Spectra from the point source and nebula region were grouped with a minimum of 50 counts per spectral channel and fitted using XSPEC. The two spectra were fitted simultaneously using absorbed non-thermal power laws with their hydrogen column density parameters linked; the results are summarized in Figure 3. The chosen model produced excellent fits ($\chi^2 = 0.9$ for 57 DoF) for a common column density of $N_H \approx 4.5(3.7 - 5.2) \times 10^{22} \text{ cm}^{-2}$ (90% confidence interval is used throughout).

The spectrum of the putative pulsar has a photon index of $\Gamma = 0.5(0.3 - 0.7)$, similar to that found for the pulsar PSR J1811–1926 in the young SNR G11.2–0.3, and at the low (hard) end of that expected for a high- \dot{E} rotation-powered pulsar ($> 4 \times 10^{36} \text{ erg s}^{-1}$; cf. Gotthelf 2003). For the PWN emission we measure a photon index of $\Gamma = 1.6(1.1 - 2.0)$, which is also at the low end for a PWN. The unabsorbed 2–10 keV fluxes for the putative PSR and PWN are $F_{PSR} = 8.8 \times 10^{-12} \text{ ergs cm}^{-2} \text{ s}^{-1}$ and $F_{PWN} = 1.0 \times 10^{-12} \text{ ergs cm}^{-2} \text{ s}^{-1}$, respectively. These results are consistent with the *ASCA* composite spectrum, having photon index $\Gamma = 0.8$, $N_H = 4 \times 10^{22} \text{ cm}^{-2}$,

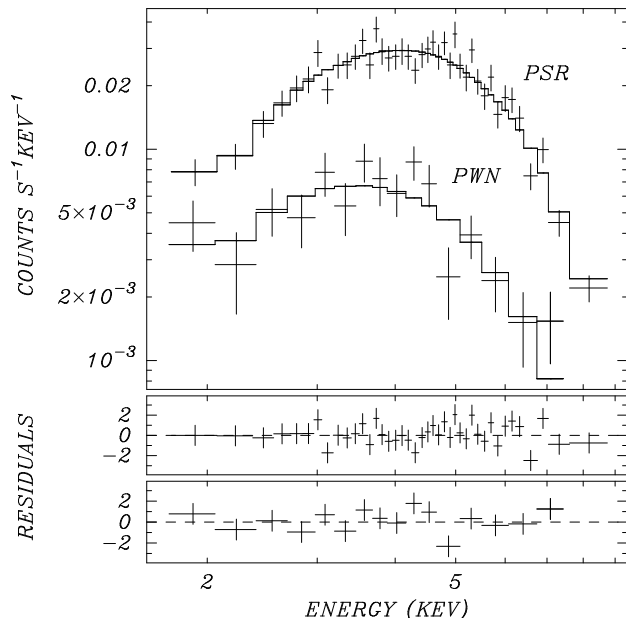


FIG. 3.— *Chandra* ACIS spectra of PSR J1838–0655 and its nebula, comprising AX J1838.0–0655, both fitted to an absorbed power-law model (see text). Residuals for each spectrum are shown in units of standard deviation.

and $F(0.7–10 \text{ keV}) = 1.1 \times 10^{-11} \text{ ergs cm}^{-2} \text{ s}^{-1}$ (Bamba et al. 2003). The flux ratio $F_{\text{PWN}}/F_{\text{PSR}} = 0.11$ is at the low end of the distribution of PWNe observed by *Chandra*, which range from 0.1–10 as compiled by Kargaltsev & Pavlov (2008).

The *Chandra* position of the point source rules out the optical/IR candidate suggested by Landi et al. (2006) on the basis of a less accurate *Swift* position. We determine an optical upper limit of $R > 23.0$ from an image obtained on the 2.4m Hiltner telescope of the MDM Observatory (Fig. 4). One does not expect to detect a pulsar having the large distance and extinction implied by the fitted N_{H} in an optical image of this depth.

2.2. AX J1837.3–0652

In addition to AX J1838.0–0655, a fainter point source (number 1 in Table 1) of 17 photons is surrounded by a large, diffuse nebula. It is evidently also a pulsar/PWN system. This source was detected by *ASCA* (AX J1837.3–0652; Bamba et al. 2003), with a 0.7–10 keV flux of $1.8 \times 10^{-12} \text{ ergs cm}^{-2} \text{ s}^{-1}$, and by *Swift* (sources 6 and 7 of Landi et al. 2006). It is difficult to measure here due to its low surface brightness. It is more extended than AX J1838.0–0655 (see Figs. 1 and 2) but has comparable total nebular flux, $\approx 1.2 \times 10^{-12} \text{ ergs cm}^{-2} \text{ s}^{-1}$ (unabsorbed) in the 2–10 keV band. Unlike AX J1838.0–0655, in AX J1837.3–0652 the PWN flux dominates over the (putative) pulsar point source. Its spectral parameters are largely unconstrained, with $0.7 < \Gamma < 3.6$ and $N_{\text{H}} = (2–12) \times 10^{22} \text{ cm}^{-2}$. If AX J1838.0–0655 is to be advanced as the origin of HESS J1837–069, then it cannot be ruled out that the PWN AX J1837.3–0652 makes a significant contribution.

2.3. Additional *Chandra* X-ray Sources

Sources 16–18 of Table 1 lie in the northeast corner of the *Chandra* image, and are evidently associated with the W42 star forming region, with source 17 being the central O5.5 star in the cluster (Blum et al. 2000). Three additional sources (numbers 2, 4, and 12) are also stars, which is consistent with their softer X-ray spectra. HD 171999 in particular is a high-proper-motion star. Its optical position listed in Table 1 is calculated for the epoch of the *Chandra* observation. None of the other sources have optical/IR counterparts in the Digitized Sky Survey or 2MASS; they are probably active galactic nuclei.

Positions for radio sources denoted by GPSR5 designations in Table 1 are measured from the 1.4 GHz VLA Multi-Array Galactic Plane Survey (White et al. 2005; Helfand et al. 2006)². The two radio sources nearest the TeV emission (numbers 8 and 10) were discussed by Figer et al. (2006) and Trejo & Rodríguez (2006). The latter authors proved that they are extragalactic based on the kinematics of their H I absorption spectra. Their X-ray positions coincide with compact components of the radio sources, presumably their host galaxy nuclei or quasars. We have no reason to hypothesize that any of these sources are related to HESS J1837–069.

3. RXTE OBSERVATIONS AND RESULTS

The point-source flux measured by *Chandra* in AX J1838.0–0655 is sufficient that a pulsar search with *RXTE* (Bradt et al. 1993) was deemed feasible. Accordingly, we requested six observations in total, pointed at AX J1838.0–0655, that spanned 2008 February 17–March 5 UT to search for the expected pulsar signal and develop a phase-connected timing solution. A log of the observations is given in Table 2. The data used here were

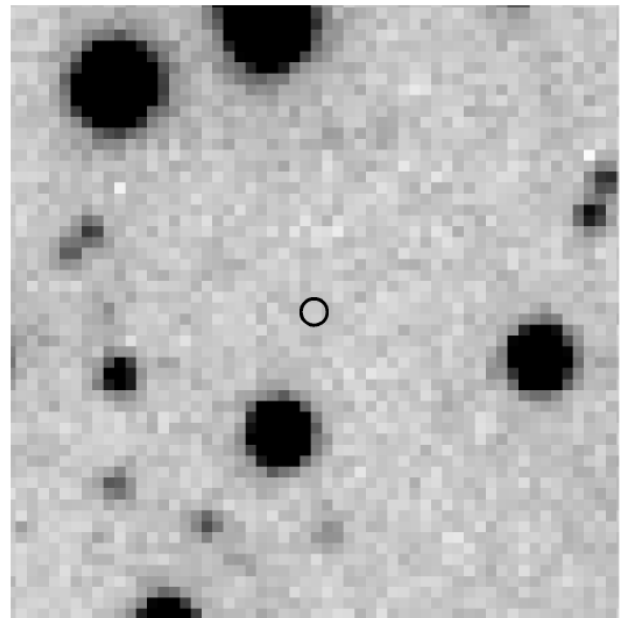


FIG. 4.— A 600 s *R*-band exposure of the center of AX J1838.0–0655 obtained on the 2.4m Hiltner telescope on 2005 July 3. The displayed field is $30'' \times 30''$. North is up, and east is to the left. The *Chandra* position of PSR J1838–0655 is indicated by a circle of radius $0.7''$, approximately its 2σ uncertainty. The magnitude limit is $R = 23.0$.

² See <http://third.ucllnl.org/gps/>.

TABLE 2
LOG OF RXTE OBSERVATIONS AND PERIOD MEASUREMENTS

Date (UT)	Exp./Span (ks)	Start Epoch (MJD)	Period ^a (ms)	Z_1^2
2008 Feb 17	9.1/14.0	54513.825	70.49820(3)	277
2008 Feb 19	20.1/35.0	54515.476	70.498218(6)	726
2008 Feb 22	5.4/8.0	54518.609	70.49828(8)	153
2008 Feb 26	5.5/8.2	54522.004	70.49823(6)	186
2008 Mar 2	5.3/8.0	54527.378	70.49829(6)	223
2008 Mar 5	6.3/8.6	54530.185	70.49830(6)	206

^aPeriod derived from a Z_1^2 test. The Leahy et al. (1983) uncertainty on the last digit is in parentheses.

collected with the Proportional Counter Array (PCA; Jahoda et al. 1996) in the GoodXenon mode with an average of 3.6 out of the five proportional counter units (PCUs) active. In this mode, photons are time-tagged to 0.9 μ s and have an absolute uncertainty better than 100 μ s (Rots et al. 1998). The effective area of five combined detectors is about 6500 cm² at 10 keV with a roughly circular field-of-view of $\sim 1^\circ$ FWHM. Spectral information is available in the 2–60 keV energy band with a resolution of $\sim 16\%$ at 6 keV.

Standard time filters were applied to the realtime PCA data, which rejects intervals of South Atlantic Anomaly passages, Earth occultations, and other periods of high particle activity. Our data contained several short (~ 200 s) intervals of detector arcing which were excised. The realtime data required manually adjusting the good data intervals to properly correspond to actual data collection times for each PCU. Table 2 lists the net exposure times and total spans of each data set. The photon arrival times were transformed to the solar system barycenter in Barycentric Dynamical Time (TDB) using the JPL DE200 ephemeris and the *Chandra* measured coordinates.

3.1. Timing Analysis

We restricted the analyzed data to the 2–20 keV energy range (PCA channels 2–50) from the top Xenon layer of each PCU to optimize the signal-to-noise. A Fast Fourier Transform (FFT) of the first observation (February 17) revealed a significant signal of power $S = 117$ at a period of $P = 70.498$ ms³. For the 5.7×10^6 search elements this corresponds to essentially nil false detection probability. There is no doubt that PSR J1838–0655 is the compact object in AX J1838.0–0655, given the morphological evidence from *Chandra* and because AX J1838.0–0655 is the brightest known X-ray source in the *RXTE* field of view.

Based on the strength of the signal in the February 17 and 19 detections of PSR J1838–0655, the next four observations were scheduled from February 22 - March 5 to develop a fully phase-coherent timing solution including the previous data sets. For each epoch, we extracted the pulse profile corresponding to the peak period as deter-

³ While planning these observations, the signal was first found by C. Markwardt (personal communication) in summed FFTs of hundreds of short, serendipitous *RXTE* dwells on the source taken during 2004–2008. However, the individual ~ 100 s exposures did not contain sufficient statistics to accurately measure the period or derive an ephemeris.

TABLE 3
TIMING PARAMETERS OF PSR J1838–0655

Parameter	Value
R.A. (J2000) ^a	18 ^h 38 ^m 03.13 ^s
Decl. (J2000) ^a	−06°55′33.4″
Epoch (MJD TDB)	54522.00000012
Period, P (ms)	70.498243969(54)
Period derivative, \dot{P}	$4.925(29) \times 10^{-14}$
Range of timing solution (MJD)	54513–54530
Characteristic age, τ_c (kyr)	22.7
Spin-down luminosity, \dot{E} (ergs s ^{−1}) ..	5.5×10^{36}
Surface dipole magnetic field, B_s (G)	1.9×10^{12}

NOTE. — TEMPO 1σ uncertainties given in parentheses.

^aChandra ACIS-I position from Table 1.

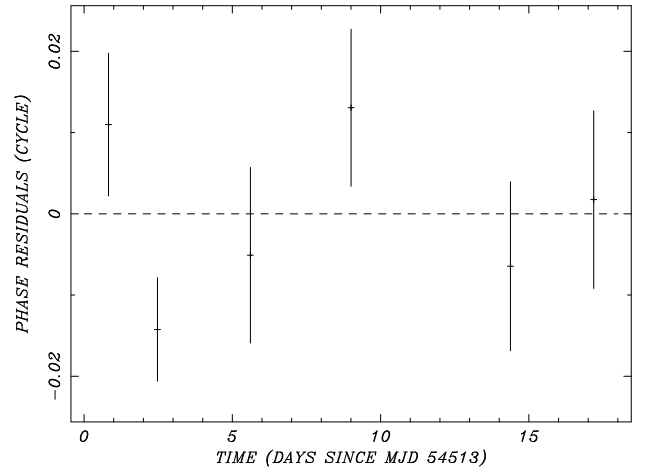


FIG. 5.— Phase residuals of the six observations of PSR J1838–0655 from the quadratic ephemeris of Table 3.

mined by the Z_1^2 test (Buccheri et al. 1983). The resulting profiles were cross correlated, shifted, and summed to generate a master pulse profile template. Individual profiles were then cross correlated with the template to determine the time of arrival (TOA) and its uncertainty in phase at each epoch. These TOAs were iteratively fitted to a quadratic ephemeris using the TEMPO software. We started by fitting just TOAs from the first three epochs, which straddle the longest observation (February 19), to a linear solution, and then added the last three TOAs to the fit one at a time. At each step we found that the new TOA would match to < 0.1 cycles the predicted phase derived from the previous set. The complete resulting ephemeris is presented in Table 3, and the phase residuals are shown in Figure 5. The residuals are all less than 0.02 cycles and appear to be random within their statistical uncertainties. Thus, inclusion of higher order terms is not indicated. An independent test of the uniqueness of the timing solution was performed using a Z_1^2 search on a two-dimensional grid of P and \dot{P} , from which we obtained consistent ephemeris parameters and errors.

Figure 6 displays the summed pulse profile using all the 2–20 keV data folded on the final ephemeris. It has a symmetric, blended double-peaked structure. The measured pulsed fraction of 4.8% indicates a intrinsic

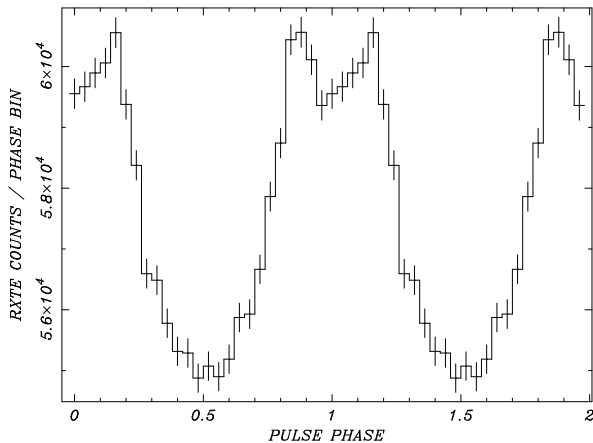


FIG. 6.— *RXTE* folded light curve of PSR J1838–0655 in the 2–20 keV band. Phase zero corresponds to the epoch of the ephemeris in Table 3.

modulation of $\gtrsim 50\%$ after allowing for the estimated internal and Galactic background in the PCA. We see no energy dependence of the pulse profile when subdividing the 2–20 keV band.

The spin-down parameters of PSR J1838–0655, particularly its $\dot{E} = 5.5 \times 10^{36}$ ergs s^{-1} , are in accord with expectation from the *Chandra* results on AX J1838.0–0655 described in §2. Assuming a distance of 6.6 kpc as discussed in §4 the ratio $L_x(2-10 \text{ keV})/\dot{E} = 8 \times 10^{-3}$ for the pulsar, and 1×10^{-3} for its PWN. The 20–300 keV flux of AX J1838.0–0655 measured by *INTEGRAL* (9×10^{-11} ergs $cm^{-2} s^{-1}$; Malizia et al. 2005) corresponds to a luminosity of $0.09 \dot{E} d_{6.6}^2$, and the > 200 GeV flux from HESS J1837–069 (3.3×10^{-11} ergs $cm^{-2} s^{-1}$; Aharonian et al. 2006a) corresponds to $0.03 \dot{E} d_{6.6}^2$.

3.2. *RXTE* Spectral Analysis

The spectrum of the pulsed flux from PSR J1838–0655 can be isolated using phase-resolved spectroscopy. We used the *fasebin* software to construct phase-dependent spectra based on the ephemeris of Table 3. For each epoch and PCU we constructed spectra from the top Xenon layer only and combined them to produce single spectra per PCU for the entire set of observations. Similarly, standard PCA responses for each PCU were generated at each epoch and averaged. In fitting the pulsed flux, the unpulsed emission provides a near perfect background estimate. The spectra were divided into two groups of 0.5 cycles each to represent the “off-peak” and “on-peak” emission and were fitted in the 2–20 keV range using XSPEC. The spectra from the four active PCUs were analyzed, both separately and combined into a single spectrum, which gave similar results.

A simple absorbed power-law model was used with the interstellar absorption held fixed at $N_H = 4.5 \times 10^{22}$ cm^{-2} determined from the *Chandra* fit; leaving the N_H unconstrained results in a larger uncertainty in Γ . The resulting best-fit photon index is $\Gamma = 1.2(1.1-1.3)$. The unabsorbed 2–10 keV pulsed flux is 9×10^{-12} ergs $cm^{-2} s^{-1}$, which represents, within statistics, all of the point-source flux of PSR J1838–0655 measured by *Chandra* (8.8×10^{-12} ergs $cm^{-2} s^{-1}$), indicating that its intrinsic pulsed fraction is $\sim 100\%$. The corresponding pulsed

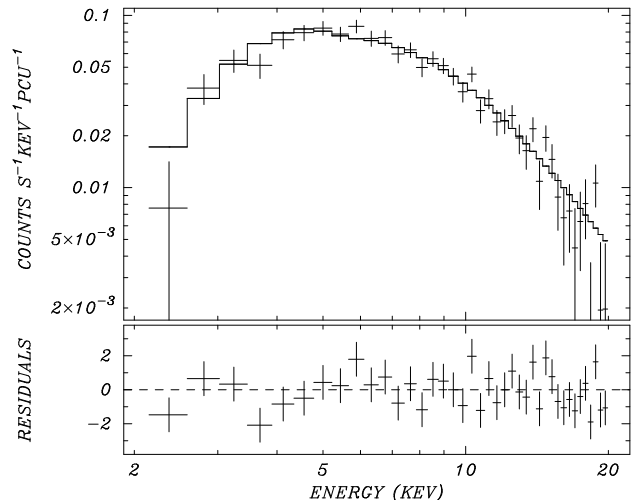


FIG. 7.— *RXTE* spectrum of pulsed flux from PSR J1838–0655 obtained by subtracting the off-peak spectrum from the on-peak spectrum, and fitting to an absorbed power-law model (see text).

luminosity (assumed isotropic) is $4.6 \times 10^{34} d_{6.6}^2$ ergs s^{-1} .

The *RXTE* power-law slope derived from the pulsed emission is slightly flatter than $\Gamma = 1.5$ reported by Malizia et al. (2005) for the joint fit to *ASCA* and *INTEGRAL* spectra of AX J1838.0–0655. We also find that this result is at odds with the *Chandra* spectra presented in §2.1, which indicate $\Gamma = 0.5 \pm 0.2$ for the dominant pulsar component. The difference is sufficiently significant to suggest that a steepening of the spectrum of the pulsar occurs in the 8–15 keV band.

4. DISCUSSION

Graphic evidence of the relationship of AX J1838.0–0655 to HESS J1837–069 is provided by the *Chandra* ACIS-I image, which resolves AX J1838.0–0655 into a point source plus a centrally peaked $2'$ diameter nebula near one end of the major axis of the TeV source. Interestingly, a second pulsar/PWN system is evident in the *Chandra* image corresponding to a weaker source previously detected as AX J1837.3–0652. Although AX J1837.3–0652 contains a point-source component ~ 100 times weaker than that of AX J1838.0–0655, the nebular fluxes of the two sources are virtually identical. This is not too surprising, as the ratio of pulsar X-ray luminosity to spin-down power is such a widely ranging quantity (Kargaltsev & Pavlov 2008). The mere presence of the second PWN is of relevance here because it indicates another likely energetic pulsar of $\dot{E} > 4 \times 10^{36}$ ergs s^{-1} (Gotthelf 2003), which implies that the two sources are *a priori* comparably suited to powering the TeV emission. Since AX J1837.3–0652 is located near the opposite end of the elongated TeV source from AX J1838.0–0655, the possibility that HESS J1837–069 comprises two PWNs, perhaps born in the same star cluster, is an intriguing question for further investigation.

The location of AX J1838.0–0655 near an unusual cluster of red supergiant stars (RSGC1; Figer et al. 2006) suggests a distance of 6.6 kpc that Davies et al. (2008) determined from the radial velocity of the cluster. Davies et al. also measured the infrared extinction to the clus-

ter, $A_K = 2.6$ mag, which is equivalent to $A_V = 23.5$, or $N_H = 4 \times 10^{22} \text{ cm}^{-2}$ according to the conversion $N_H/A_V = 1.79 \times 10^{21} \text{ cm}^{-2} \text{ mag}^{-1}$ (Predehl & Schmitt 1995). Our X-ray fitted N_H is consistent with this. It is plausible that PSR J1838–0655 was born in this young cluster, which is centered 3' north-northwest of the X-ray source (see Figure 1). At this distance, a 23 kyr old neutron star born in the center of the cluster requires a transverse velocity of 245 km s^{-1} to reach its present location, less if it was born in the outskirts.

It is possible that the TeV PWN is displaced in one direction from the pulsar by an asymmetric reverse shock resulting from a supernova that exploded initially in an inhomogeneous medium, an explanation suggested by Blondin et al. (2001) for the similar appearance of the Vela X remnant (Aharonian et al. 2006b). Other likely associations that show such displacements are PSR B1823–13/HESS J1825–137 (Aharonian et al. 2006c; Pavlov et al. 2008), PSR J1809–1917/HESS J1809–193 (Aharonian et al. 2007; Kargaltsev & Pavlov 2007), PSR J1718–3825/HESS J1718–385 (Aharonian et al. 2007; Hinton et al. 2007), and possibly PSR J1617–5055/HESS J1616–508 (Aharonian et al. 2006a; Landi et al. 2007).

Based on the number of red supergiants in the cluster RSGC1, Davies et al. (2008) estimate that it has a total mass of $(2 - 4) \times 10^4 M_\odot$, the highest of any young cluster in the Galaxy. Figer et al. (2006) calculated that it should produce a supernova every 40–80 kyr on average, which is frequent enough statistically to expect a pulsar of the 23 kyr characteristic age that we measured for AX J1838.0–0655. In fact, it is statistically suggestive that the previous pulsar born in this cluster is AX J1837.3–0652, and that it contributes to HESS J1837–069. Theoretically, TeV sources powered by pulsars can live for up to 100 kyr as inverse Compton emitters in regions of low (μG) B -fields (de Jager & Djannati-Atai 2008).

A plausible mechanism of the TeV emission from HESS J1837–069 is inverse Compton scattering of ambient photons off relativistic electrons in an extended PWN, with the target IR/optical photons supplied by the star cluster. Considering the luminosity of only the IR detected supergiants of RSGC1 as a lower limit on the seed photons ($\approx 2.8 \times 10^6 L_\odot$; Figer et al. 2006; Davies et al. 2008), at a distance of $3 \times 10^{19} \text{ cm}$ from the cluster the energy density of optical/IR photons in HESS J1837–069 is $\sim 20 \text{ eV cm}^{-3}$. If the pulsar injected $10^{37} \text{ e}^\pm \text{ s}^{-1}$ into this region for the past 10^4 yr with average $\gamma = 10^6$, then the inverse Compton luminosity can be $\leq 2.7 \times 10^{36} \text{ ergs s}^{-1}$. This approximation does not account for the Klein-Nishina suppression of the cross section, which would reduce it. Nevertheless, it appears sufficient to supply the $1.7 \times 10^{35} d_{6.6}^2 \text{ ergs s}^{-1}$ luminosity of HESS J1837–069, as it does not even invoke the higher luminosity from the pulsar in its younger phase, which energy may still be present as relic electrons in the extended TeV nebula.

5. CONCLUSIONS

Using *Chandra*, we resolved the X-ray image and spectrum of AX J1838.0–0655 into its pulsar and PWN components, with 2–10 keV luminosities of $L_{PSR} = 4.6 \times 10^{34} d_{6.6}^2 \text{ ergs s}^{-1}$ and $L_{PWN} = 5.2 \times 10^{33} d_{6.6}^2 \text{ ergs s}^{-1}$. Led by this evidence we searched for pulsations using *RXTE* and discovered PSR J1838–0655 in AX J1838.0–0655 at a period of 70.5 ms. Timing its spin-down, we found $\dot{E} = 5.5 \times 10^{36} \text{ ergs s}^{-1}$, a value that is consistent with pulsars of similar X-ray luminosity and X-ray nebular properties. The 20–300 keV luminosity observed by *INTEGRAL* (Malizia et al. 2005) is $\approx 4.7 \times 10^{35} d_{6.6}^2 \text{ ergs s}^{-1}$, and is likely to be an extension of the hard pulsar spectrum rather than the PWN. The 0.2–20 TeV luminosity of HESS J1837–069 is $1.7 \times 10^{35} d_{6.6}^2 \text{ ergs s}^{-1}$, which is 3% of the pulsar \dot{E} , while the TeV emission is several times larger in extent than the X-ray PWN. PSR J1838–0655 is located at one end of the elongated TeV source.

The 23 kyr characteristic age of PSR J1838–0655 is comparable to those of the middle-aged pulsars Vela and PSR B1823–13, with which it shares the characteristic of an X-ray PWN displaced from the center of a larger TeV nebula. Such pulsars are old enough that the displacement can be enforced by a reverse supernova shock propagating in an inhomogeneous interstellar medium. Alternatively or in addition, we may be seeing relic electrons from asymmetric diffusion out of the PWN in an earlier phase.

We also discovered a *Chandra* point source inside a second diffuse X-ray source adjacent to HESS J1837–069. Probably an older pulsar/PWN, AX J1837.3–0652 may also contribute to HESS J1837–069, explaining its elongated shape as a blended source. This scenario may be testable with spatially resolved spectroscopy of the TeV emission, especially if the age of the putative second pulsar is significantly different from the first. Although not yet conclusively identified as a pulsar, AX J1837.3–0652 should have similar spin-down luminosity as AX J1838.0–0655. A deep search for radio pulsations from AX J1837.3–0652 is warranted to determine its spin-down parameters, it being too faint for an X-ray search.

We thank the *RXTE* mission for making observing time available for this project. We are especially grateful to Drs. Jean Swank and Craig Markwardt for their invaluable assistance in planning these observations. This work also made use of archival data from the *Chandra* X-ray Observatory Center. Financial support was provided by the National Aeronautics and Space Administration through *Chandra* Award SAO G08-9060X issued by the *Chandra* X-ray Observatory Center, which is operated by the Smithsonian Astrophysical Observatory for and on behalf of NASA under contract NAS8-03060.

REFERENCES

- Aharonian, F., et al. 2005, *Science*, 307, 1938
 ———. 2006a, *ApJ*, 636, 777
 ———. 2006b, *A&A*, 448, L43
 ———. 2006c, *A&A*, 460, 365
 ———. 2007, *A&A*, 472, 489
 Bamba, A., Ueno, M., Koyama, K., & Yamauchi, S. 2003, *ApJ*, 589, 253

- Blondin, J. M., Chevalier, R. A., & Frierson, D. M. 2001, *ApJ*, 563, 806
- Blum, R. D., Conti, P. S., & Damineli, A. 2000, *AJ*, 119, 1860
- Bradt, H. V., Rothschild, R. E., & Swank, J. H. 1993, *A&AS*, 97, 355
- Buccheri, R., et al 1983, *A&A*, 128, 245
- Burke, B. E., Gregory, J., Bautz, M. W., Prigozhin, G. Y., Kissel, S. E., Kosicki, B. N., Loomis, A. H., & Young, D. J. 1997, *IEEE Trans. Electron Devices*, 44, 1633
- Davies, B., Figer, D. F., Law, C. J., Kudritzki, R.-P., Najarro, F., & Herrero, A., & MacKenty, J. W. 2008, *ApJ*, 676, 1016
- de Jager, O. C., & Djannati-Atai, A. 2008, in *Neutron Stars and Pulsars: 40 Years After Their Discovery*, ed. W. Becker, Springer Lecture Notes, in press (arXiv:0803.0116)
- Figer, D. F., MacKenty, J. W., Robberto, M., Smith, K., Najarro, F., Kudritzki, R. P., & Herrero, A. 2006, *ApJ*, 643, 1166
- Funk, S. 2007, *Ap&SS*, 309, 11
- Gotthelf, E. V. 2003, *ApJ*, 591, 361
- Helfand, D. J., Becker, R. H., White, R. L., Fallon, A., & Tuttle, S. 2006, *AJ*, 131, 2525
- Hertz, P., & Grindlay, J. E. 1988, *AJ*, 96, 233
- Hinton, J. A., Funk, S., Carrigan, S., Gallant, Y. A., de Jager, O. C., Kosack, K., Lemièrre, A., & Pühlhofer, G. 2007 *A&A*, 476, L25
- Jahoda, K., Swank, J. H., Giles, A. B., Stark, M. J., Strohmayer, T., Zhang, W., & Morgan, E. H. 1996, *Proc. SPIE*, 2808, 59
- Kargaltsev, O., & Pavlov, G. G. 2007, *ApJ*, 670, 655
- . 2008, in *40 Years of Pulsars: Millisecond Pulsars, Magnetars, and More*, eds. C. Basa, A. Cumming, V. M. Kaspi, & Z. Wang, ASP Conf. Proc., in press (arXiv:0801.2602)
- Landi, R., Bassani, L., Malizia, A., Masetti, N., Stephen, J. B., Bazzano, A., Ubertini, P., Bird, A. J., & Dean, A. J. 2006, *ApJ*, 651, 190
- Landi, R., de Rosa, A., Dean, A. J., Bassani, L., Ubertini, P., & Bird, A. J. 2007, *MNRAS*, 380, 926
- Leahy, D. A., Eisner, R. F. & Weisskopf, M. C. 1983, *ApJ*, 272, 256
- Malizia, A., et al. 2005, *ApJ*, 630, L157
- Monet, D. G., et al. 2003, *AJ*, 125, 984
- Pavlov, G. G., Kargaltsev, O., & Brisken, W. F. 2008, *ApJ*, 675, 683
- Predehl, P., & Schmitt, J. H. M. M. 1995, *A&A*, 293, 889
- Rots, A. H., et al. 1998, *ApJ*, 501, 749
- Trejo, A., & Rodríguez, L. F. 2006, *Rev. Mex. AA*, 42, 147
- White, R. L., Becker, R. H., & Helfand, D. J. 2005, *AJ*, 130, 586